Wavelet Spatio-Temporal Change Detection on multi-temporal SAR images

Rodney V. Fonseca, Rogério G. Negri, Aluísio Pinheiro, and Abdourrahmane Atto, *Senior Member, IEEE*

***Abstract*—We introduce WECS (Wavelet Energies Correlation Screening), an unsupervised procedure to detect spatio-temporal change points on multi-temporal SAR images. The procedure is based on wavelet approximation for the multi-temporal images, wavelet energy apportionment, and ultra-high dimensional correlation screening for the wavelet coefficients. We show WECS performance on simulated multi-temporal image data. We also evaluate the proposed method on a time series of 84 satellite images in a forest region at the border of Brazil and the French Guiana. The proposed method displays good results in covering change regions, with the additional benefit of having simple and fast computation.**

***Index Terms*—Change detection, Remote Sensing, multi-temporal images, simulated images, wavelets.**

I. Introduction

CHANGE detection is an important task performed in remote sensing image that allows researchers and engineers to identify and evaluate modifications on land surfaces captured by multi-temporal satellite images. Analyzing problems such as deforestation [1], rapid urbanization [2] and glacier melting [3] are of great importance to study the dynamics of regions sensitive to climate changes and human activity. Furthermore, the increase on availability of satellite images in the past years raises the challenge of applying computationally cheap methods to images available at larger and larger from time to time. A review for change detection in multi-temporal remote sensing is given by [4].

Most methods used for change detection analysis can be classified either as supervised (training data is used to set up the method) or unsupervised (fully data-driven techniques). We shall focus in this work on unsupervised approaches, whose examples in the literature include the works of [5]–[10]. Many other proposals of methods vary in their motivations as well as in their applicability. Change detection in multi-temporal hyperspectral images is discussed in [11]–[13]. [14] pursue change detection techniques via non-local means and principal component analysis. Compressed projection and image fusion are employed by [15]. Deep learning by slow feature analysis for change detection is the subject of [16]. [17] proposes a change detection method driven by adaptive parameter estimation.

A special attention has been given for multi-temporal change detection using Synthetic Aperture Radar (SAR) images. Some of the references already mentioned are examples of change detection methods applied to SAR images [1]–[3], [7], [14], [15], [18] . Known to be not affected by weather, cloud and sunlight conditions, SAR images rise as an essential data source in change detection applications [18]. Conversely, due to its acquisition architecture, the speckle noise typically affects the images obtained by SAR sensors and demands additional pre-processing before its use.

Face with the complexity imposed by the high-dimensionality of multi-temporal datasets in addition to the presence of speckle noise, the change detection process using SAR images becomes a challenge task. In this context, the use of Wavelets rises as a convenient approach once such technique is robust when dealing with noise data and is allows an efficient computational treatment.

In more details, Wavelet methods present many advantages for a plethora of statistical applications [19] not only in remote sensing problems thanks to wavelet capabilities in capturing multi-scale/resolution information. Their computational efficiency and sparseness are specially relevant for large images and other high-dimensional data [20]. Analysis of SAR images have been investigated under different approaches using wavelet methods, such as [21], [22], [23], [24]. However, an application of screening ideas on wavelet coefficients is still a novel approach in change detection literature, and we show it has an interesting potential to provide good results even with simple algorithms.

In the light of presented discussions and motivations, using Wavelet and data screening concepts, we propose the Wavelet Energies Correlation Screening (WECS), a novel unsupervised multi-temporal change detection method for SAR images. The main idea behind WECS is built on ultra-high dimensional feature screening for the wavelet coefficients [25]. Such method is usually employed in high-dimensional regression models to reduce the problem's dimension by subsetting the available covariates in such a way that true covariates are among the chosen ones with high probability [26]. We show that by applying the feature screening idea on multi-temporal images, we obtain a fast and accurate method to cover change regions with good detection rates.

This paper is organized as follows: Section III introduces the problem and presents the proposed method. We show WECS performance on simulated multi-temporal image data in Section **??**. In Section **??** we apply the proposed method to a time

This work was supported by FAPESP grants 2016/24469-6 and 2018/04654-9 and CNPq grants 309230/2017-9 and 310991/2020-0.

R. Fonseca and A. Pinheiro are with the Department of Statistics, University of Campinas, Campinas 13083-859, Brazil (e-mails: ra192588@dac.unicamp.br; pinheiro@ime.unicamp.br).

A. Atto is with the LISTIC - Polytech Annecy-Chambéry, Université de Savoie, 74944 Annecy le Vieux Cedex, France (e-mail: Abdourrahmane.Atto@univ-savoie.fr).

R. G. Negri is with the Department of Environmental Engineering, São Paulo State University, São José dos Campos, Brazil (e-mail: rogerio.negri@unesp.br).

series of 85 satellite images in the border region of Brazil and the French Guiana, for images captured from November 08, 2015 to December 09 2017. Section V concludes the paper with a discussion.

II. Basic Theory Background

Wavelet methods have been widely applied to analyze images in signal processing literature, specially for tasks such as signal denoising and compression [27]. The most common way of describing wavelet representations is as a multi-resolution decomposition, where a signal is represented on approximation and detail coefficients, which provide coarse and finer details of the signal, respectively. In practice, the discrete wavelet transform of matrices (image) consists in applying low and high-pass convolution filters to its rows and columns [28]. In case of smoothing, applying such low-pass filter J times to rows and columns of a matrix $\mathcal{I}$, yields a smooth image $\mathbf{X}$. The number J is also called resolution level, a tuning parameter for wavelet smoothing. This wavelet smoothing is employed in the next section as a denoising step for image analysis.

Using wavelet smoothing on the images consists in an initial step to analyze the data, but the main goal in the analysis is to find changes in space and at instants of time. The smoothed images still contain a large number of coefficients that need to be evaluated simultaneously, what characterizes a high-dimensional problem with multiple time series corresponding to each location in space. We need to employ a method that retains the most important locations driving overall modifications across time. This type of problem is recurrent in statistics, and particularly in regression analysis it is mainly recognized as a variable selection problem. Methods like variable selection are largely employed to identify the most important covariates in a study, and one method particularly efficient in identifying relevant variables when the number of candidates is very large is the feature screening technique.

Feature screening procedure is a method originally designed for ultra-high dimensional regression models [26]. In order to explain how it works, consider the usual linear regression framework where $\mathbf{y}$ is a $n \times 1$ vector of observations from a response variable and $\{\mathbf{W}_1 \cdots \mathbf{W}_p\}$ is a $n \times p$ matrix with explanatory variables on its columns, which are used in a linear model $\mathbf{y} = \sum_{i=1}^{p} \beta_i \mathbf{W}_i + \boldsymbol{\epsilon}$, where $\beta_1, \ldots, \beta_p$ are unknown parameters and $\boldsymbol{\epsilon}$ is a zero mean random noise. The problem setup is that p is much larger than n, what makes standard regression methods unfeasible, but only a handful of the available covariates are relevant for the model, i.e., have a nonzero corresponding parameter β_i. The feature screening idea consists in computing the sample correlation $\mathrm{corr}(\mathbf{y}, \mathbf{W}_i)$ among response and explanatory variables, and then selecting those covariates whose correlation are among the highest values. Under suitable conditions, such method is known to select a set containing all true covariates with high probability. In the image change detection problem, our idea is that a similar approach could be used to detect change locations by taking an overall change measure as response variable and local (pixel) measures as potential covariates.

III. Wavelet Energy Correlation Screening

Figure 1 depicts a high-level conceptualization for the proposed method. The elements included in such representation are formalized in the constructions as follows.

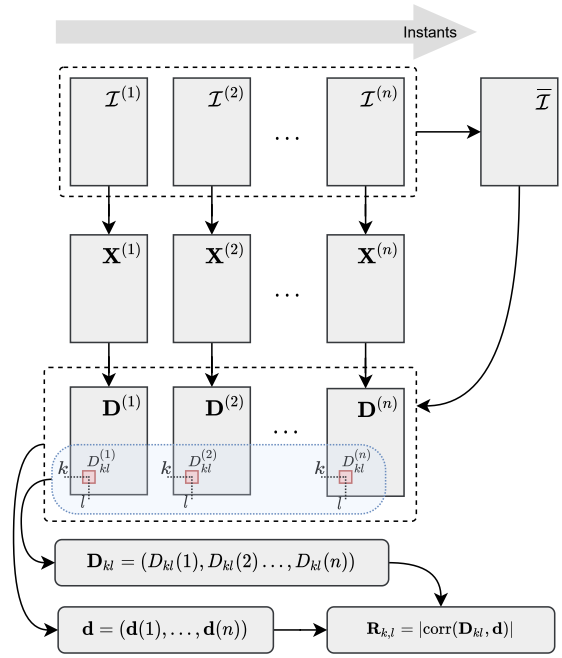

Fig. 1. Diagram of steps performed on WECS to compute an absolute correlation of a single point.

Let $\mathcal{I}^{(1)}, \ldots, \mathcal{I}^{(n)}$ be an image time series defined on a support $\mathcal{S} = \{1, \ldots, u\} \times \{1, \ldots, v\} \subset \mathbb{N}^2$, hence representing a region of interest over n distinct instants. These images may be relative to one SAR channel or a combination of channels; this will be specified when appropriate. Our goal is twofold: to find possible points in time where some relevant changes might have taken place at the region represented in $\mathcal{I}^{(m)}$, $m = 1, \ldots, n$, and to find which regions are closely associated to the observed changes along time. We shall address these tasks by analyzing the bidimensional stationary discrete wavelet decomposition of $\mathcal{I}^{(m)}$. Stationary wavelets (also known as non-decimated or redundant wavelets) is a traditional de-noising method that can be efficiently applied to two-dimensional signals such as images [21], [29], [30].

After application of this wavelet transform to $\mathcal{I}^{(m)}$ at some appropriate resolution level $J \geq 1$, one of its by-products is a matrix of so called approximation wavelet coefficients $\mathbf{X}^{(m)}$, a smoothed version of $\mathcal{I}^{(m)}$ defined on the same support $\mathcal{S}$. The higher $J \in \{1, \ldots, \log_2(\min u, v)\}$ is, the smoother $\mathbf{X}^{(m)}$ gets.

Beyond many other aspects that can be involved in wavelet analysis of images, which may include different types of wavelet transform and basis as well the use of thresholding for detail coefficients, the current construction is focused on $\mathbf{X}^{(m)}$ to provide a simple wavelet smoothing. Nevertheless, extensions based on distinct aspects are straightforward.

We can then consider further apportioning the total $\mathbb{L}_2$ energy of the series $\left\{\mathbf{X}^{(m)}\right\}_{m=1,\ldots,n}$ as:

$$\sum_{m=1}^{n} \|\mathbf{X}^{(m)}\|_F^2 = n\|\overline{\mathcal{I}}\|_F^2 + 2n\langle\overline{\mathbf{X}} - \overline{\mathcal{I}}, \overline{\mathcal{I}}\rangle_F + \sum_{m=1}^{n} \|\mathbf{X}^{(m)} - \overline{\mathcal{I}}\|_F^2, \tag{1}$$

where $\overline{\mathcal{I}} = n^{-1}\sum_{m=1}^{n}\mathcal{I}^{(m)}$ and $\overline{\mathbf{X}} = n^{-1}\sum_{m=1}^{n}\mathbf{X}^{(m)}$; $\|\cdot\|_F$ and $\langle\cdot,\cdot\rangle_F$ represents the Frobenius norm and inner product, respectively. Naturally, both $\overline{\mathcal{I}}$ and $\overline{\mathbf{X}}$ share the support $\mathcal{S}$.

The most right-hand term in Equation (1) measures the deviations between the wavelet coefficients at distinct instants ($\mathbf{X}^{(m)};\ m = 1,\ldots,n$) regarding the *average image* (i.e., $\overline{\mathcal{I}}$). Such deviations may favor detecting relevant changes over the time. Since each element (i.e., a pixel/position $(k,l) \in \mathcal{S}$) of $\mathbf{X}^{(m)}$ also has a corresponding sequence of deviations in time, the local deviation to the overall measure may also allow detecting the spatial changes. Among several approaches able to detect change events, the Pearson correlation coefficient rises as an convenient alternative. Furthermore, such measure shares connections with the idea of feature screening employed in high-dimensional regression, as explained earlier.

Let $X_{kl}^{(m)}$ and $\overline{\mathcal{I}}_{kl}$ be the entry (k,l) of $\mathbf{X}^{(m)}$ and $\overline{\mathcal{I}}$, respectively. The matrix $\mathbf{D}^{(m)}$ embraces the squared differences between $\mathbf{X}^{(m)}$ and $\overline{\mathcal{I}}$, where $D_{kl}^{(m)} = \left(\mathbf{X}_{kl}^{m} - \overline{\mathcal{I}}_{kl}\right)^2$. Therefore, it is defined the temporal overall variation sequence $\left\{\mathbf{d}^{(m)}\right\}_{m=1,\ldots,n}$, whose elements are given by:

$$\mathbf{d}(m) = \sum_{k=1}^{u}\sum_{l=1}^{v} D_{kl}^{(m)} \tag{2}$$

In this context, an instant m in $\left\{\mathbf{d}^{(m)}\right\}_{m=1,\ldots,n}$ with high value stands for the image $\mathcal{I}^{(m)}$ where the most expressive changes take place.

In order to identify spatio-temporal changes, we employ the concept of ultra-high dimensional correlation screening [25] discussed in Section II. For each local squared deviation time series given by individual elements of $\mathbf{D}^{(m)}$ across $m = 1,\ldots,n$, say $\mathbf{D}_{kl} = \left\{D_{kl}^{(1)},\ldots,D_{kl}^{(n)}\right\}$, consider the absolute value of its Pearson correlation with the overall squared deviations, given by $\mathbf{d}$:

$$R_{kl} = |\mathrm{corr}\left(\mathbf{D}_{kl},\mathbf{d}\right)|.$$

Consequently, rises the matrix $\mathbf{R}$ from the elements R_{kl} assigned to each $(k,l) \in \mathcal{S}$.

Let us define a mapping of *important* indices for changes over the image series with respect to $\overline{\mathcal{I}}$ as $\mathcal{M}^\star \subseteq \mathcal{S}$ where *changes in* $\{\mathcal{I}^{(m)}\}_{m=1,\ldots,n}$ *with respect to* $\overline{\mathcal{I}}$ *are affected by local changes in the images*.

An empirical mapping of change locations may be stated by:

$$\mathcal{M}_\tau = \{(k,l) \in \mathcal{S} : |R_{kl}| > \tau\}, \tag{3}$$

where $\tau \in \mathbb{R}_+^*$ is a convenient threshold value. The idea is that for suitable values of τ, the empirical set $\mathcal{M}_\tau$ has high probability of detecting the correct change locations in $\mathcal{M}^\star$ [25]. This screening idea has been successfully applied in different problems in areas such as graphical models [31], time series [32] and remote sensing [33]. We show it can also shed light on problems related to change point detection in time series of images.

IV. Experiments

A. Experiment design

In order to assess the proposed method, this section presents two distinct studies comprising distinct datasets.

The first study (Sec. IV-B) uses a simulated data set and focus on identify the most appropriated wavelet family and resolution level J. Specifically, the Haar (haar), Daubechies of order 2 and 4 (db2 and db4), Coiflets of order 4 (coif4) and Symlets of order 2 and 4 (sym2 and sym4) wavelet families are analyzed [34], [35]. Posterior, once selected the wavelet family, the most suitable resolution level is then pointed out.

Lastly, the performance of the proposed method is measured in terms of True/False Positive Ratios and Receiver Operating Characteristic (ROC) curve. Comparisons with the standard Thresholding of Aggregate Absolute Difference (TAAD) and a non-wavelet version of WECS, herein called Energy Correlation Screening (ECS), are included in the experiments.

In summary, the TAAD comprises the application of a thresholding algorithm on the accumulated change representation image $\mathbf{A}$ where $A_{kl} = \sum_{m=2}^{n}|\mathcal{I}_{kl}^{(m)} - \mathcal{I}_{kl}^{(m-1)}|$. The ECS stands for the use of $\mathcal{I}^{(m)}$ instead of $\mathbf{X}^{(m)}$ when defining $D_{kl}^{(m)}$ at Equation 2.

The second study (Sec. IV-C) analyzes the performance of WECS, and respective comparison with TAAD and ECS, in a real-world application with actual SAR image series. The appropriate wavelet family and resolution level previously identified are employed. ROC curves, F1-Score [36], the kappa coefficient, and the variance of kappa [37], are adopted for this purpose. Additionally, the computational run-times are presented and discussed.

B. Simulated data analysis

This section applies the WECS, TAAD, and ECS methods to detect changes on a simulated multi-temporal image dataset. Such series comprises 80 multi-temporal images and it is synthesized by repeating a sequence of four images with different types of changes plus a noise. Examples of the first four instants are shown in Figure 2. These images/instants are generated by summing two matrices: (i) a binary signal matrix with ones denoting where the ellipses occur and zero elsewhere; (ii) and a noise matrix with random variables following a standard Gaussian distribution.

The first image, $\mathcal{I}^{(1)}$, presents three elongated ellipses. The second image $\mathcal{I}^{(2)}$ has shorter and larger ellipses added. Smaller ellipses are then added to form $\mathcal{I}^{(3)}$ and $\mathcal{I}^{(4)}$. All the changes made that occur among subsequent images are shown in Figure 3(a), where white regions (i.e., the "ones") correspond to changes along with the instants.

Applying WECS to these images, we obtain a matrix $\mathbf{R}$ of correlations between deviations of each $\mathcal{I}$ entry with the total squared mean deviation. An example of $\mathbf{R}$ is presented in Figure 3(b). For some choice of threshold τ on absolute values of $\mathbf{R}$, we obtain a binary matrix that can be compared with the total true changes shown in Figure 3(a). Similarly, Figures 3(c) and 3(d) depicts the matrices $\mathbf{A}$ and $\mathbf{R}$ provided by TAAD and ECS methods.

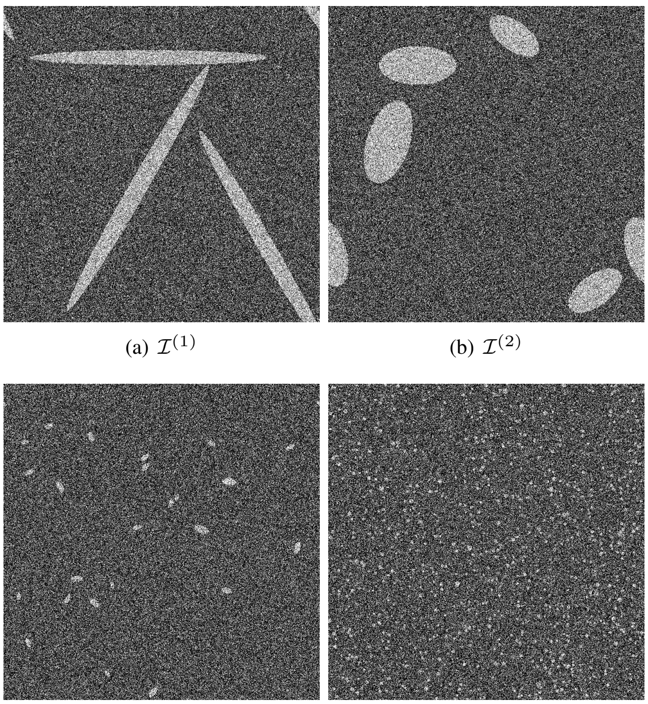

(a) $\mathcal{I}^{(1)}$ (b) $\mathcal{I}^{(2)}$

(c) $\mathcal{I}^{(3)}$ (d) $\mathcal{I}^{(4)}$

Fig. 2. Example of the first four simulated multi-temporal images. Features and changes come as white ellipses and dots.

According to the experiment design (Section IV-A), ROC curves are employed to compare the performance of each analyzed method and inspect the effects of both J and wavelet basis on the performance of the WECS method. In summary, the ROC curves exhibit the performance as a function of true and false positive ratios when distinguishing two events (in this context, the change and non-changed pixels/positions) using distinct thresholds. The true and false positive ratios are computed using the "total change" image (Fig. 3(a)) as reference. Moreover, the tested thresholds embrace all values in $\mathbf{R}$ (or $\mathbf{A}$), excluding repetitions and considering it in ascending order.

Figure 4(a) presents the ROC curves considering distinct wavelet basis in the WECS method. All instances adopts $J = 2$. The curves allow concluding that db2 and sym2 deliver the best trade-off between true and false positive ratios (i.e., high true positive ratios even when the false positive ratios are low). As a consequence of this finding, all the following experiments and analyses consider the db2 wavelet basis.

Figure 4(b) depicts the ROC curves with $J \in \{1, 2, 3, 4, 5\}$ as decomposition levels. The profiles exhibited by the ROC curves make evident that J equal to 2 or 3 promotes the best performances, with a slight advantage for $J = 2$, since it demands few decomposition levels. The overall performance

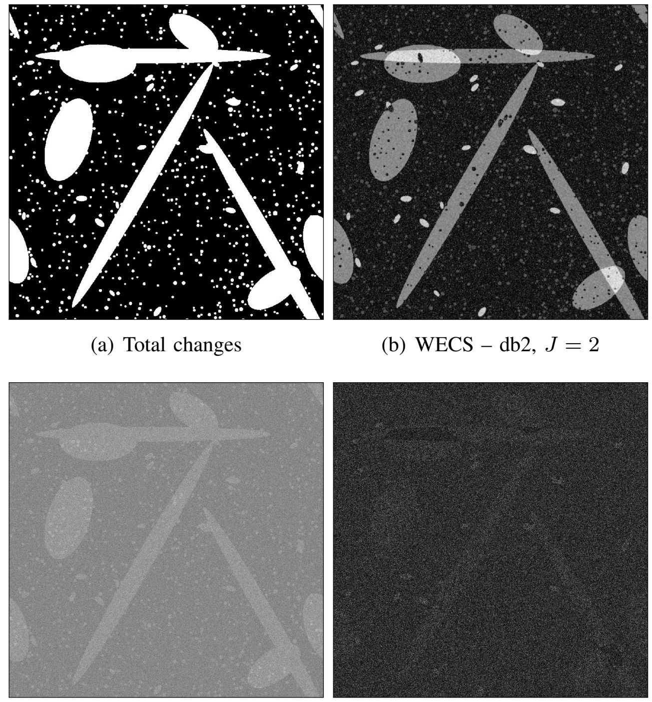

(a) Total changes (b) WECS – db2, $J = 2$

(c) TAAD – $\mathbf{A}$ (d) ECS

Fig. 3. Expected change/non-change regions and typical results provided bu WECS, TAAD and ECS before the thresholding process.

for $J = 2$ warrants its use for the rest of the comparisons.

At last, the ROC curves shown in Figure 4(c) allow comparing the performances of WECS, TAAD and ECS approaches. Firstly, the low-performance assigned to the ECS method allows concluding that the simple swap of the wavelet transform by a "deviation image" into the proposed correlation screening pipeline is an inconvenient choice and reinforces the importance of the wavelet smoothing in the context of the proposed method. About the performance of TAAD method, a true positive ratio of 0.8 is guaranteed when tolerating a false positive ratio of approximately 0.4. Reversely, the WECS method provides the same true positive ratio under an almost nill false positive ratio, demonstrating then its superiority compared to the competitors.

C. Actual remote sensing application

We employed the proposed change detection method on a series of 84 multi-date satellite images. The images were taken on a forest region at the border of Brazil and the French Guiana from 2015-12-26 to 2017-12-3. Each image has two channels (VV and VH) and 1538 by 1556 pixels. We perform a change detection wavelet analyses on the combined image by considering each observed entry as $\mathcal{I}_{k,l}^{(m)} = ((\mathrm{VV}_{k,l}^{(m)})^2 + (\mathrm{VH}_{k,l}^{(m)})^2)^{1/2}$, where VV and VH represent the matrices of observations from VV and VH channels, respectively.

A multi-resolution analysis based on a Symlet basis with filter of length 16 (symlet 8) is built. In order to have dimensions as power of 2, the matrices $\mathcal{I}_{k,l}$ are extended to a 2048×2048 matrix with $\mathcal{I}_{k,l}$ at the center and the remaining parts being completed with mirrored values at the borders. The

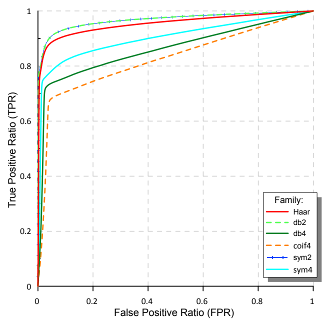

(a) $\mathbf{d}(m)$ with different wavelet bases and J=2

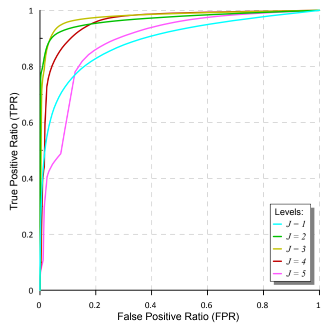

(b) db2 $\mathbf{d}(m)$ with different levels

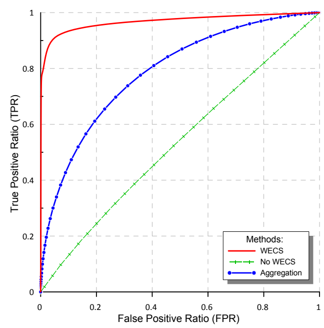

(c) The proposed methods in black (db2 WECS $\mathbf{d}(m)$) vs two non-wavelet methods: standard log-ratio aggregation (red stars); and $\mathbf{d}(m)$ (blue)

Fig. 4. ROC curves for detection of changing ellipses in simulated images and different methods.

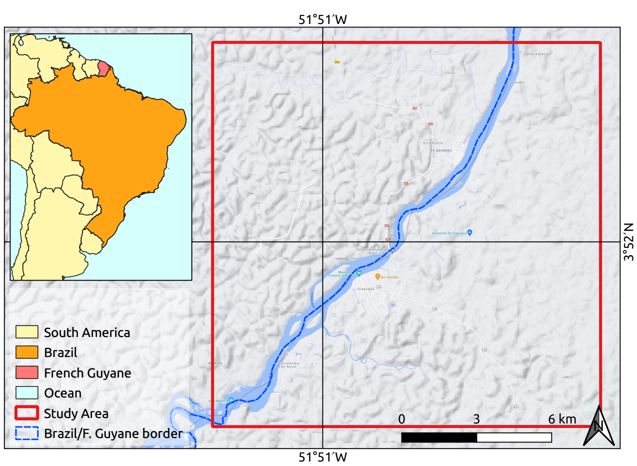

Fig. 5. Study area location. (preliminar)

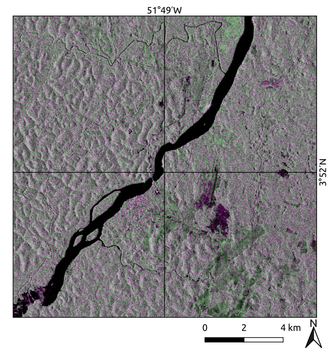

(a) 26th December, 2015

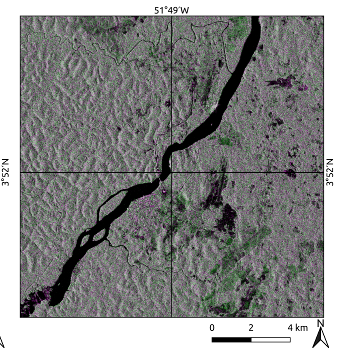

(b) 3rd December, 2017

(c) Ground truth change/non-change samples

Fig. 6. Inserir caption...

wavelet transform at resolution level $J = 2$ is applied to these matrices and only the portion corresponding to the 1538×1556 is kept for further processing. Then, we are able to compute the squared mean differences vector $\mathbf{d}$ and the matrix of absolute correlations $\mathbf{R}$.

The time change measures computed with $\mathbf{d}$ are shown in Figure 7. The orange line in Figure 7a represents the median absolute deviation of $\mathbf{d}$, which allow us to notice times that differ expressively from the others. We can notice that times $m = 25, 27, 30$ are highlighted as having the most expressive changes. The images corresponding to these times can be seen in Figure 8.

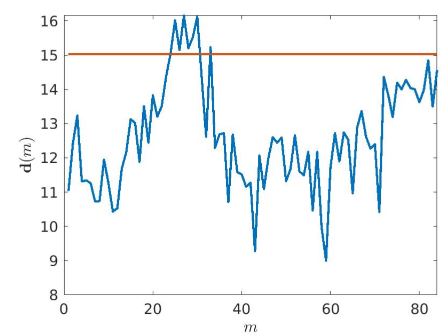

Fig. 7. Plot of $\mathbf{d}(m)$, $m = 1, \ldots, 85$ with orange horizontal line indicating two times its median absolute deviation.

The changes in space can be analyzed using the image obtained with $\mathbf{R}$, which is displayed in Figure 7c. Denoting the images' dimension as $N = 1538 \times 1556$, if we take the $[N/\log N]$ largest absolute correlations as those corresponding to possible change points, we obtain a matrix of zeros and ones that is presented in Figure 7e. The white regions in Figure 7c (entries with value one) represent the change points, which seem to concentrate mainly on three regions: at the center, to the right of the river; at the top, on the left border of the river; and at the top left. Computing aggregated absolute differences to measure changes in space, we obtain Figure 7d. An image of detected changes corresponding to measures in Figure 7d can be obtained applying a thresholding method for grayscale images. Figure 7f shows the result of using Otsu's thresholding method [38] for aggregation of absolute differences.

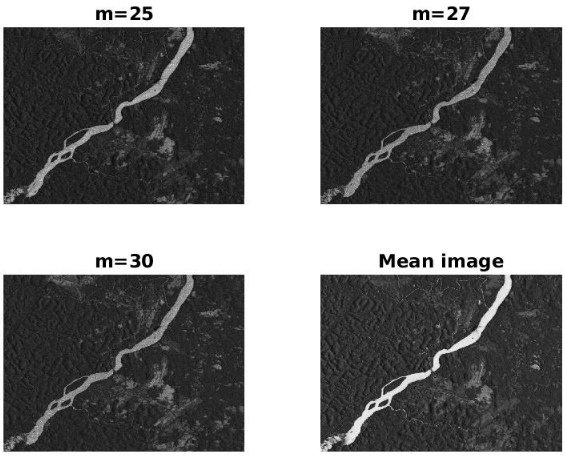

Fig. 8. Images $\mathbf{X}^{(m)}$ from times m correspond to top-3 highest values of $\mathbf{d}(m)$ and the mean image $\bar{\mathcal{I}}$.

The comparison of performance for the two change detection measures considered here can be checked in Figure 9, where a ROC curve is computed to check the correct detection of changes. WECS attains high true positive rates before the aggregation method, but both methods design competitive results. This performance differs from the ROC curve results in the previous section because the real images have a mean signal to noise ratio (SNR) of 3.9327, whereas the simulated images were generated with SNR of 0.2309. Hence, WECS is expected to have performance closer to the aggregation method in less noisy applications. The reference of correct change regions is shown in Figure 9a, which are determined using [XXXXX].

We can also compare the change detection methods using the F_1-score accuracy measure. Denoting TP as the number of true positives (change pixels correctly detected), FP as the number of false positives (nonchange pixels flagged as change point) and FN as the total of false negatives (change points flagged as nonchange point), the F_1-score is defined as

$$F_1 = 2\frac{\mathrm{Pr}\cdot\mathrm{Re}}{\mathrm{Pr}+\mathrm{Re}},$$

where

$$\mathrm{Pr} = \frac{\mathrm{TP}}{\mathrm{TP}+\mathrm{FP}} \quad \text{and} \quad \mathrm{Re} = \frac{\mathrm{TP}}{\mathrm{TP}+\mathrm{FN}}.$$

Results of these three accuracy measures are presented in Table I. Results for aggregation of absolutes differences correspond to two types of thresholds: Otsu's method and Kittler-Illingworth [39]. We can observe that WECS presents the highest value of F_1-score, which means it has a better performance that the competing method.

V. Discussion

We present a novel way of detecting changes in multi-temporal satellite images, WECS. The procedure is based on wavelet energies from both the estimated individual coefficients as well as the whole mean image. It makes use of correlation screening for ultra-high dimensional data. Thereupon, WECS is expected to provide a sample of points in space in a way that such set, contains real change points with high probability. The proposed method's performance is shown using both simulated and real data. The proposed method is useful to detect spatio-temporal change points, which is illustrated on data analyses. The method is employed to analyze a time series of 84 images of a forest.

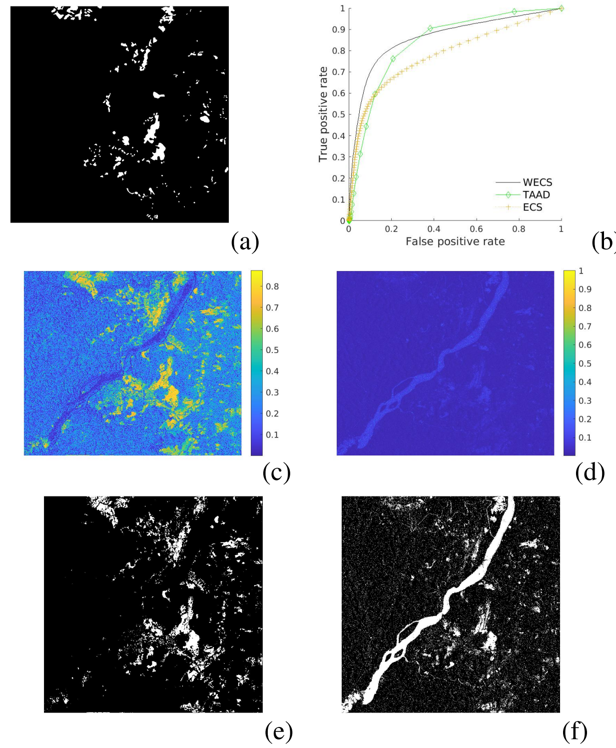

Fig. 9. Change points in space of the forest data. (a) Regions (in white) where changes should be detected. (b) ROC curve for detection of changing regions. (c) Matrix of absolute correlations obtained with WECS. (d) Change measures from aggregation of absolute differences. (e) Change regions detected by highlighting the $[N/\log N]$ largest correlations in $\mathbf{R}$ (N denoting the image's dimension). (f) Change regions detected using aggregated absolute differences and Otsu's thresholding.

TABLE I
Accuracy measures F_1-score, Precision (Pr) and Recall (Re) computed from detection of changing regions in the forest data using WECS (taking the $[N/\log N]$ largest correlations as corresponding to change) and the aggregation of absolute differences with Otsu and Kittler-Illingworth's (KI) thresholds.

	Aggregated - Otsu	Aggregated - KI	WECS
F_1-score	0.2231	0.2163	0.3253
Pr	0.1369	0.1296	0.2390
Re	0.6022	0.6526	0.5094

References

[1] T. L. Barreto, R. A. Rosa, C. Wimmer, J. B. Nogueira, J. Almeida, and F. A. M. Cappabianco, "Deforestation change detection using high-resolution multi-temporal X-band SAR images and supervised learning classification," in *2016 IEEE International Geoscience and Remote Sensing Symposium (IGARSS)*. Beijing, China: IEEE, 2016, pp. 5201–5204.

[2] Y. Ban and O. A. Yousif, "Multitemporal spaceborne SAR data for urban change detection in China," *IEEE Journal of Selected Topics in Applied Earth Observations and Remote Sensing*, vol. 5, no. 4, pp. 1087–1094, 2012.

[3] C. Scher, N. C. Steiner, and K. C. McDonald, "Mapping seasonal glacier melt across the Hindu Kush Himalaya with time series synthetic aperture radar (SAR)," *The Cryosphere*, vol. 15, no. 9, pp. 4465–4482, 2021.

[4] Y. Ban and O. Yousif, "Change detection techniques: A review," in *Multitemporal Remote Sensing*, Y. Ban, Ed. Cham: Springer, 2016, pp. 19–43.

[5] L. Bruzzone and D. F. Prieto, "Automatic analysis of the difference image for unsupervised change detection," *IEEE Transactions on Geoscience and Remote Sensing*, vol. 38, no. 3, pp. 1171–1182, 2000.

[6] T. Celik, "Change detection in satellite images using a genetic algorithm approach," *IEEE Geoscience and Remote Sensing Letters*, vol. 7, no. 2, pp. 386–390, 2010.

[7] G. Quin, B. Pinel-Puyssegur, J.-M. Nicolas, and P. Loreaux, "MIMOSA: An automatic change detection method for SAR time series," *IEEE Transactions on Geoscience and Remote Sensing*, vol. 52, no. 9, pp. 5349–5363, 2014.

[8] S. Saha, F. Bovolo, and L. Bruzzone, "Change detection in image time-series using unsupervised LSTM," *IEEE Geoscience and Remote Sensing Letters*, 2020.

[9] R. G. Negri, A. C. Frery, W. Casaca, S. Azevedo, M. A. Dias, E. A. Silva, and E. H. Alcântara, "Spectral–spatial-aware unsupervised change detection with stochastic distances and support vector machines," *IEEE Transactions on Geoscience and Remote Sensing*, vol. 59, no. 4, pp. 2863–2876, 2021.

[10] R. G. Negri and A. C. Frery, "Unsupervised change detection driven by floating references: A pattern analysis approach," *Pattern Analysis and Applications*, vol. 24, 2021.

[11] F. Bovolo and L. Bruzzone, "The time variable in data fusion: A change detection perspective," *IEEE Geoscience and Remote Sensing Magazine*, vol. 3, no. 3, pp. 8–26, 2015.

[12] S. Liu, D. Marinelli, L. Bruzzone, and F. Bovolo, "A review of change detection in multitemporal hyperspectral images: Current techniques, applications, and challenges," *IEEE Geoscience and Remote Sensing Magazine*, vol. 7, no. 2, pp. 140–158, 2019.

[13] T. Matsunaga, A. Iwasaki, S. Tsuchida, K. Iwao, J. Tanii, O. Kashimura, R. Nakamura, H. Yamamoto, S. Kato, K. Obata, K. Mouri, and T. Tachikawa, "Current status of hyperspectral imager suite (HISUI) onboard International Space Station (ISS)," in *2017 IEEE International Geoscience and Remote Sensing Symposium (IGARSS)*. Fort Worth, USA: IEEE, 2017, pp. 443–446.

[14] M. Jia and L. Wang, "Novel class-relativity non-local means with principal component analysis for multitemporal SAR image change detection," *International Journal of Remote Sensing*, vol. 39, no. 4, pp. 1068–1091, 2018.

[15] B. Hou, Q. Wei, Y. Zheng, and S. Wang, "Unsupervised change detection in SAR image based on Gauss-log ratio image fusion and compressed projection," *IEEE Journal of Selected Topics in Applied Earth Observations and Remote Sensing*, vol. 7, no. 8, pp. 3297–3317, 2014.

[16] B. Du, L. Ru, C. Wu, and L. Zhang, "Unsupervised deep slow feature analysis for change detection in multi-temporal remote sensing images," *IEEE Transactions on Geoscience and Remote Sensing*, vol. 57, no. 12, pp. 9976–9992, 2019.

[17] Y. Chen, Z. Ming, and M. Menenti, "Change detection algorithm for multi-temporal remote sensing images based on adaptive parameter estimation," *IEEE Access*, vol. 8, pp. 106 083–106 096, 2020.

[18] F. Bovolo and L. Bruzzone, "A detail-preserving scale-driven approach to change detection in multitemporal SAR images," *IEEE Transactions on Geoscience and Remote Sensing*, vol. 43, no. 12, pp. 2963–2972, 2005.

[19] B. Vidakovic, *Statistical Modeling by Wavelets*. New York: John Wiley & Sons, 1999.

[20] P. A. Morettin, A. Pinheiro, and B. Vidakovic, *Wavelets in Functional Data Analysis*. Cham: Springer, 2017.

[21] A. M. Atto, E. Trouvé, Y. Berthoumieu, and G. Mercier, "Multidate divergence matrices for the analysis of SAR image time series," *IEEE Transactions on Geoscience and Remote Sensing*, vol. 51, no. 4, pp. 1922–1938, 2012.

[22] N. Bouhlel, G. Ginolhac, E. Jolibois, and A. Atto, "Multivariate statistical modeling for multi-temporal SAR change detection using wavelet transforms," in *2015 8th International Workshop on the Analysis of Multitemporal Remote Sensing Images (Multi-Temp)*. Annecy, France: IEEE, 2015, pp. 1–4.

[23] T. Celik, "Multiscale change detection in multitemporal satellite images," *IEEE Geoscience and Remote Sensing Letters*, vol. 6, no. 4, pp. 820–824, 2009.

[24] S. Cui and M. Datcu, "Statistical wavelet subband modeling for multi-temporal SAR change detection," *IEEE Journal of Selected Topics in Applied Earth Observations and Remote Sensing*, vol. 5, no. 4, pp. 1095–1109, 2012.

[25] J. Fan, R. Li, C.-H. Zhang, and H. Zou, *Statistical Foundations of Data Science*. Boca Raton: CRC Press, 2020.

[26] J. Fan and J. Lv, "Sure independence screening for ultrahigh dimensional feature space," *Journal of the Royal Statistical Society: Series B*, vol. 70, no. 5, pp. 849–911, 2008.

[27] S. G. Mallat, *A Wavelet Tour of Signal Processing*. San Diego: Academic Press, 1998.

[28] ——, "A theory for multiresolution signal decomposition: the wavelet representation," *IEEE transactions on pattern analysis and machine intelligence*, vol. 11, no. 7, pp. 674–693, 1989.

[29] R. R. Coifman and D. L. Donoho, "Translation-invariant de-noising," in *Wavelets and statistics*, A. Antoniadis and G. Oppenheim, Eds. New York: Springer, 1995, pp. 125–150.

[30] A. M. Atto, E. Trouvé, J.-M. Nicolas, and T. T. Lê, "Wavelet operators and multiplicative observation models—application to SAR image time-series analysis," *IEEE Transactions on Geoscience and Remote Sensing*, vol. 54, no. 11, pp. 6606–6624, 2016.

[31] Z. Zheng, H. Shi, Y. Li, and H. Yuan, "Uniform joint screening for ultra-high dimensional graphical models," *Journal of Multivariate Analysis*, vol. 179, p. 104645, 2020.

[32] K. Yousuf and Y. Feng, "Targeting predictors via partial distance correlation with applications to financial forecasting," *Journal of Business & Economic Statistics*, pp. 1–13, 2021.

[33] X. Li, H. Lin, J. Long, and X. Xu, "Mapping the growing stem volume of the coniferous plantations in North China using multispectral data from integrated GF-2 and Sentinel-2 images and an optimized feature variable selection method," *Remote Sensing*, vol. 13, no. 14, p. 2740, 2021.

[34] G. Beylkin, R. Coifman, and V. Rokhlin, "Fast wavelet transforms and numerical algorithms i," *Communications on Pure and Applied Mathematics*, vol. 44, no. 2, pp. 141–183, 1991.

[35] I. Daubechies, *Ten Lectures on Wavelets*. USA: Society for Industrial and Applied Mathematics, 1992.

[36] C. J. V. Rijsbergen, *Information Retrieval*, 2nd ed. USA: Butterworth-Heinemann, 1979.

[37] R. G. Congalton and K. Green, *Assessing the accuracy of remotely sensed data: principles and practices*, 3rd ed. CRC press, 2019.

[38] N. Otsu, "A threshold selection method from gray-level histograms," *IEEE Transactions on Systems, Man, and Cybernetics*, vol. 9, no. 1, pp. 62–66, 1979.

[39] J. Kittler and J. Illingworth, "Minimum error thresholding," *Pattern Recognition*, vol. 19, no. 1, pp. 41–47, 1986.